An integrated hydrogen isotopes transport model for the TRIEX-II facility

2. TRIEX-II loop

As highlighted before, the Gas/Liquid Contactor (GLC), in particular the packed column technology, was selected to be tested and qualified in TRIEX-II facility at ENEA Brasimone Research Centre, Italy.

TRIEX-II presents a ring design, as shown in Fig. 1. The recirculation tank S100 contains the LiPb eutectic alloy and acts also as a draining tank. The liquid metal is pumped by means of a permanent magnet pump EP100. Then, it is sent towards the saturator S200, which to ensures the complete Q_2 solubilization (hydrogen and deuterium are used instead of tritium, as detailed in the next paragraph) until the equilibrium concentration is reached. Subsequently, the lithium-lead is delivered to the extractor column S300 through a pipeline equipped with a by-pass: in this way, a supplementary lithium-lead flow rate control can be accomplished by balancing extraction and saturation with the aim of reaching a stable steady-state condition. In the packed tower mock-up, the extraction of the hydrogen isotopes from the eutectic LiPb is mediated by a purge gas flow of helium, G, which is flushed in counter-current with respect to the liquid phase flow of lithium-lead (L).

Two operational modes are foreseen. In the *operational mode A*, the hydrogen is solubilized in the saturator and a stripping gas of helium is used at the extractor. In the *operational mode B*, the deuterium is solubilized in the saturator, and a mixture of helium and hydrogen is used as stripping gas in the extractor. On the one hand, the Q partial pressure in LiPb is determined by the hydrogen permeation sensors HLM733, HLM734 and HLM735. They measure the Q concentration in LiPb at the inlet of the saturator and at the inlet and outlet of the extractor. On the other hand, a quadrupole mass spectrometer, HGA, measures the Q_2 concentration in the stripping gas at the extractor outlet. This provides a way of having two different measurements of the same parameter. The main design parameters of TRIEX-II are reported in Table 1.

Table 1. Main design parameters of TRIEX-II.

Parameter	Value	Unit
Nominal LiPb mass flow rate	0.2-4.5	[kg s^{-1}]
LiPb temperature	250-530	[°C]
He vol. flow rate at saturator inlet	10-250	[Nl h^{-1}]
Max H_2 concentration at saturator inlet	5	[vol. %]
He pressure at saturator inlet	2-4	[barg]
He vol. flow rate at extractor inlet	50-250	[Nl h^{-1}]
He stripping pressure at the gas inlet	3-6	[barg]

3. Description of the model

3.1 COMSOL 2D model of the extractor

The extractor GLC mock-up was modelled in a 2D geometry, Fig. 2. The uncompressible flow was solved in terms of velocity and pressure with the $k-\varepsilon$ model; the output velocity field was used as an input for the transport model by solving a general, scalar, passive transport equation:

$$\frac{\partial c}{\partial t} + (\nabla \cdot \vec{u})c - \nabla \cdot (D\nabla c) = s \qquad (1)$$

where c [mol m^{-3}] is the tritium concentration in the specific domain (lithium-lead, vessel, filling material), $\vec{u}$ [m s^{-1}] is the velocity field of LiPb, D [m^2 s^{-1}] is the diffusion coefficient of hydrogen and s [mol m^{-3} s^{-1}] is the time-dependent molar hydrogen generation rate along the x and y directions. Although an accurate description in a CFD model of the sink term due to hydrogen extraction would require more detailed analyses (for instance, the tritium source in a liquid metal breeding blanket is calculated via Monte Carlo simulations), in this work a simplified approach was adopted. The sink term was defined, similarly to the procedure adopted in [8], as a combination of two functions, $f(x,y)$ and $g(t)$, describing the spatial and the temporal evolution, respectively:

$$s(x,y,t) = -f(x,y) \cdot g(t) \qquad (2)$$

The minus sign in Eq. (2) denotes that hydrogen was removed from the lithium-lead. The temporal evolution was derived by directly coupling the 0D Simulink model with the corresponding S-function. By doing so, the temporal trend of the sink was found. In particular, the function derived was $g(t) = 10^{-5} \cdot \exp(-t/2500)$. As far as the spatial term is concerned, a uniform distribution along the packing column was assumed, i.e. $f(x,y) = 1$.

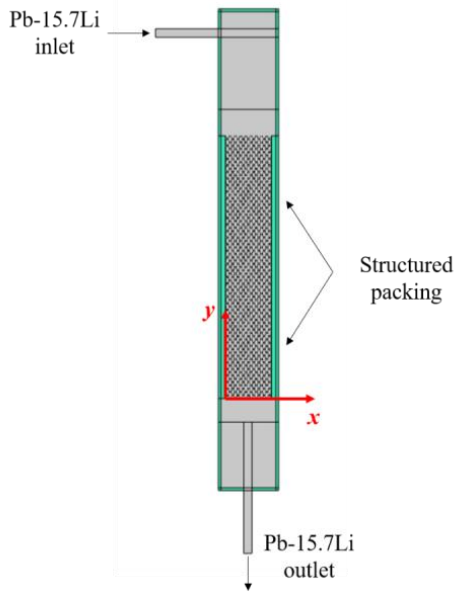

Fig. 2. Geometry of the extractor used for 2D modelling.

A diffusion-limited regime (DLR) was assumed since the permeation parameter W, calculated according to [9], is greater than 1. For the vessels and for the structured packing, $W = 3.31$ and $W = 6.57$, respectively. The assumption of a DLR is then acceptable. As far as boundary conditions are concerned, pressure continuity was imposed at the interface LiPb/steel and LiPb/filling. For the calculations, Eurofer97 properties were considered [10], due to a lack in literature regarding the steel of the piping (A 182 Gr F22) and the steel of the

vessels (2 ¼ Cr-1 Mo). This choice is fairly reasonable since they are both ferritic-martensitic steels. The structured filling of saturator and extractor is composed by 2 and 4 Sulzer MellapakPlus 452Y modules, respectively, with specific surface of 350 [m^2 m^{-3}] and realized in AISI 316L; its transport properties have been taken from [11]. The BC of pressure continuity can be synthetically written at the interfaces of Eurofer97 and MellapakPlus as:

$$c_{H,Eu} = K_{Eu/MP} \cdot c_{H,MP} \quad (3)$$

$$K_{Eu/MP} = \frac{K_{Eu/LM}}{K_{MP/LM}} = \frac{k_{S,Eu}/k_{S,LM}}{k_{S,MP}/k_{S,LM}} \quad (4)$$

where subscripts Eu, MP, LM refer to Eurofer, MellapakPlus and LiPb, respectively, K [-] is the global partition coefficient of the Eurofer domains (vessel, inlet and outlet pipes of the extractor) and of the Mellapak domain, and k_S [mol m^{-3} $Pa^{-0.5}$] is the Sieverts' constant, Table 2.

Table 2. Main input parameters for 2D model.

Param.	Description	Value	Unit
$k_{S,Eu}$	Sieverts' const. Eurofer [10]	$1.52 \cdot 10^{-3}$	[mol m^{-3} $Pa^{-0.5}$]
$k_{S,MP}$	Sieverts' const. Mellapak [11]	$5.49 \cdot 10^{-2}$	[mol m^{-3} $Pa^{-0.5}$]
$k_{S,LM}$	Sieverts' const. LiPb [12]	$2.39 \cdot 10^{-2}$	[mol m^{-3} $Pa^{-0.5}$]
$K_{Eu/LM}$	Part. coef. Eu/LiPb	$6.34 \cdot 10^{-2}$	[-]
$K_{MP/LM}$	Part. coef. Mp/LiPb	2.30	[-]
$K_{Eu/MP}$	Global part. coef. Eu/Mp	$2.76 \cdot 10^{-2}$	[-]
a	Specific area of the packing	350	[m^{-1}]
h_{GLC}	Height of LiPb column	1466	[mm]
h_{MP}	Total height of Mellapak filling	852	[mm]
d_{GCL}	Diameter of GLC mock-up	168.3	[mm]
t_{GCL}	Thickness of GLC vessel	8	[mm]
d_{pipe}	Int. diameter inlet/outlet pipe	25.4	[mm]
p_{H_2}	Partial pressure of hydrogen	126	[Pa]
L	Mass flow rate of LiPb	1.14	[kg s^{-1}]
G	Vol. flow rate of stripping gas	138	[Nl h^{-1}]

The global partition coefficient was evaluated as the ratio of the partition coefficient between Eurofer and LiPb domains with respect to the ratio of the partition coefficient between Mellapak and LiPb. The initial values for the lithium-lead, vessel, pipes and structured filling were derived from Sieverts' constant and from the hydrogen partial pressure in the LiPb alloy. The experimental conditions used in this simulation are summarized in Table 3.

Table 3. Experimental conditions of the test performed in TRIEX-II facility.

Param.	Description	Value	Unit
T	Operative temperature	400	[°C]
L	Mass flow rate of LiPb	1.14	[kg s^{-1}]
G	Vol. flow rate of stripping gas	138	[Nl h^{-1}]
L/G	L over G ratio	3.00	[-]
p_{H_2}	Partial pressure of hydrogen	126	[Pa]
y_{out}	Molar fraction of H_2 extracted	$3.80 \cdot 10^{-4}$	[-]

3.2 Integration in MATLAB/Simulink

The integration of the 2D COMSOL model of the extractor with the whole TRIEX-II loop was developed by means of Simulink, following the approach reported in [5]. In this way, it is possible to have a fast tool able to describe the circuit with a system level code, with the detail of the 2D sub-system constituted by the GLC mock-up.

The integration was realized throughout a customized Simulink system function, or S-Function, which was written in MATLAB code. In general, an S-function is constituted by a vector of states, x, which is connected to a vector of inputs, u, and to a vector of outputs, y. For the present application, the vector of input was constituted by the concentration at the inlet of the feeding pipe of the extractor.

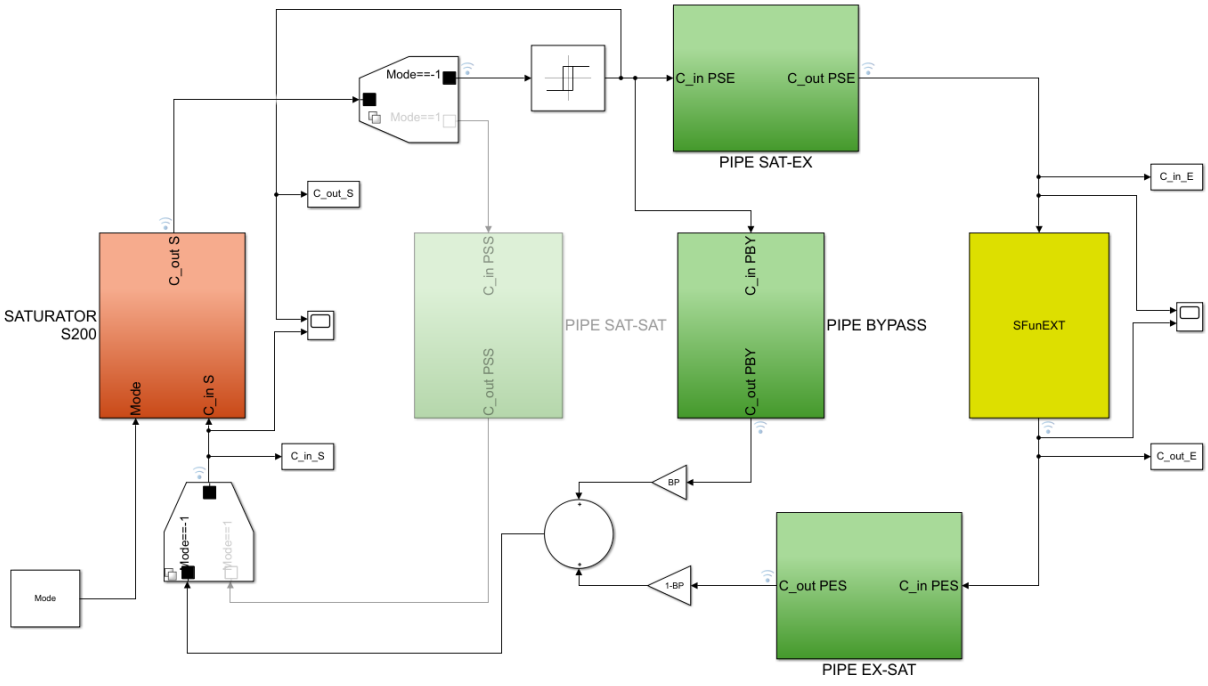

Fig. 3. Simulink model of TRIEX-II facility – extraction mode.

This describes the inlet boundary condition of the COMSOL 2D model, whereas the vector of states was solved implicitly with COMSOL solver for a certain time step; in this way, a vector of output $y = f_0(t, x, u, u_0)$ containing the average concentration in the LiPb after the hydrogen extraction to be used in the next block was created.

Such evaluation is executed by Simulink in different stages, for all the block circuit. Firstly, in the initialization phase (*mdlInitializeSizes*), Simulink initializes the model, incorporating the library blocks and evaluating the block parameters with a certain execution order. Within this phase, the time step of the Simulink simulation, *tstep*, is imported, together with the initial condition, u_0, which is represented by the inlet concentration of the COMSOL model. Then, the simulation loop starts, where the solver repeatedly executes each block in the model, according to the order established during the initialization phase. In these simulation steps, the block states are updated for the current sample time, i.e. between *t* and *tstep*, by means of the function *mdlUpdate*, which, for the present system, yields to $x_{d_{k+1}} = f_u(t, x_{d_k}, u)$, where $x = [0; x_d]$ represents the vector of discrete states. Finally, after having evaluated the block state for each COMSOL run, the output is generated and evaluated with *mdlOutputs*. The output average concentration was then used as an input for the next Simulink block.

The assessment of the Simulink blocks, Fig. 3, was carried out considering the following components:

- Pipeline (green) from saturator S200 to extractor S300;
- Pipeline (green)from saturator S200 to the end of the by-pass line;
- Pipeline (green) from extractor S300 to saturator S200;
- Pipeline (green) from saturator S200 and return to S200 (when only saturation occurs);
- The saturator S200 (red);
- The extractor S300 (yellow, S-function).

The model was constructed with the purpose of being able to operate in saturation mode (where the extractor is not considered) and in extraction mode (where saturator and extractor are both considered). In this application, the model runs in extraction mode. A mass balance equation was written for the pipes and for the saturator. Only the circuit section interested during the tests was considered, so that the storage tank S100 and the loading pipe were not considered. The permeation parameter W for the piping is 1.40. This means that the permeation regime is closed to a mixed regime. However, to simplify the calculations, the DLR was also assumed for the piping, being a conservative assumption. In this case, the following equation can be written:

$$V_p \frac{dc_{H,out}}{dt} = Q_{LM}(c_{H,in} - c_{H,out}) - \frac{\phi_p A_{lat,p}}{t_p}\sqrt{p_{H_2,in}} \qquad (5)$$

where V_p [m^3] is the internal volume of the pipe, $C_{H,in}$ [mol m^{-3}] and $C_{H,out}$ [mol m^{-3}] are hydrogen concentration in LiPb at the inlet and the outlet respectively, Q_{LM} [m^3 s^{-1}] is the lithium-lead volumetric flow rate in the pipe section, ϕ_p [mol m^{-1} s^{-1} Pa$^{-0.5}$] is the permeability of the pipe, $A_{lat,p}$ [m^2] is the lateral surface of the pipe, t_p [m] is the thickness of the pipe and $p_{H_2,in}$ [Pa] is the partial pressure of hydrogen in LiPb at the inlet. The partial pressure of hydrogen in LiPb is calculated through the Sieverts' law according to Aiello's correlation [12]. The Aiello's correlation was chosen because it is a conservative choice; moreover, in the experimental campaign, as detailed in [3], the experimental results were best represented by Aiello's correlation.

For the saturator, a similar mass balance equation was introduced:

$$V_S \frac{dc_{H,out}}{dt} = Q_{LM}(c_{H,in} - c_{H,out}) - \frac{\phi_S A_{lat,S}}{t_S}\sqrt{p_{H_2,out}} + S \qquad (6)$$

where V_S [m^3] is the internal volume of the saturator, ϕ_S [mol m^{-1} s^{-1} Pa$^{-0.5}$] is the permeability of the saturator, $A_{lat,S}$ [m^2] is the lateral surface of the saturator vessel, t_S [m] is the thickness, $p_{H_2,out}$ [Pa] is the partial pressure of hydrogen in LiPb at the outlet and S [mol m^{-3} s^{-1}] is the source term:

$$S = Q_S\,(C_{H_2,in} - C_{H_2,out}) \qquad (7)$$

where Q_S [m^3 s^{-1}] is the volumetric flow rate of gas injected into the saturator and C_{H_2} [mol m^{-3}] represents the concentration of hydrogen in the gas mixture at the inlet and at the outlet of the saturator.

Theoretically, the extraction efficiency was evaluated considering the concentration at the inlet and at the outlet of the extractor:

$$\eta = 1 - \frac{C_{H.out}}{C_{H,in}} \qquad (8)$$

From an experimental viewpoint, as detailed in Section 2, the extraction efficiency was measured by means of hydrogen permeation sensor and by means of the HGA according to the following equations:

$$\eta_S = 1 - \sqrt{\frac{p_{H_2,out}}{p_{H_2,in}}} \qquad (9)$$

$$\eta_{HGA} = \frac{2\,\rho_{LiPb}}{k_{S,A}\sqrt{p_{H_2,in}}\,M_{LiPb}}\,\frac{y_{out} - y_{in}}{L_M/G_M} \qquad (10)$$

where $p_{H_2,in}$ [Pa] and $p_{H_2,out}$ [Pa] are the pressures of the hydrogen permeated through the permeation sensors HLM734 and HLM735, respectively, ρ_{LiPb} [kg m^{-3}] is the lithium-lead density [13], $k_{S,A}$ [mol m^{-3} Pa$^{-0.5}$] is the Aiello's Sieverts' constant, M_{LiPb} [kg mol^{-1}] is the molecular weight of LiPb, y_{out} [-] is the molar fraction of hydrogen in the stripping gas at the outlet of the extractor and y_{in} [-] is the molar fraction at the inlet. The value of y_{out} is read by the HGA, whereas y_{in} is assumed to be zero.

Finally, the whole Simulink model was solved by means of a fixed-step, third-order Runge-Kutta scheme [6].

4. Results and discussion

The velocity profile in the extractor, for the operative condition listed in Table 3, is displayed in Fig. 4. The flow path results in a recirculation zone above the MellapakPlus packing, ensuring a much fine liquid metal dispersion into the structured filling. This allows a better mass transport with the passage of hydrogen isotopes from LiPb to the gas phase. The flow rate at the outlet pipe is slightly accelerated due to the Venturi effect.

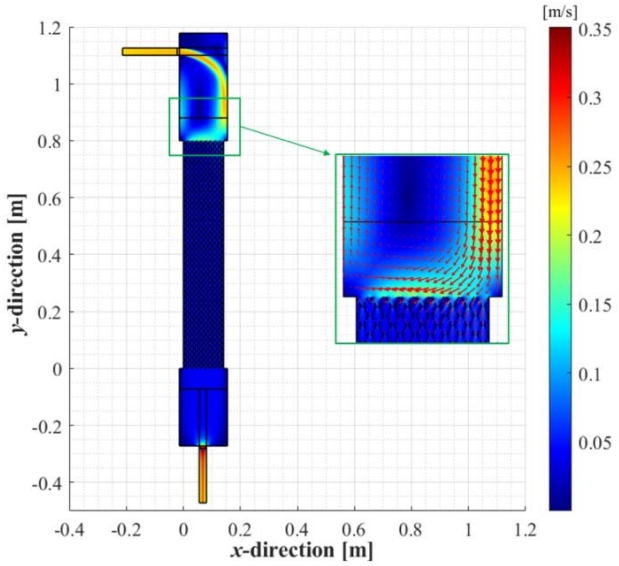

Fig. 1. Velocity field of LiPb in the extractor.

During the experimental campaign, the hydrogen solubilized in the saturator was accurately kept constant in order to balance the hydrogen extracted by the GLC mock-up. In this way, the extraction efficiency was constant. To simulate this behaviour in the Simulink model, a relay has been inserted after the saturator. The concentrations at the extractor inlet and outlet and the extraction efficiency of the model are reported in Fig. 5 and compared with the experimental efficiencies evaluated with Eqs. 9-10.

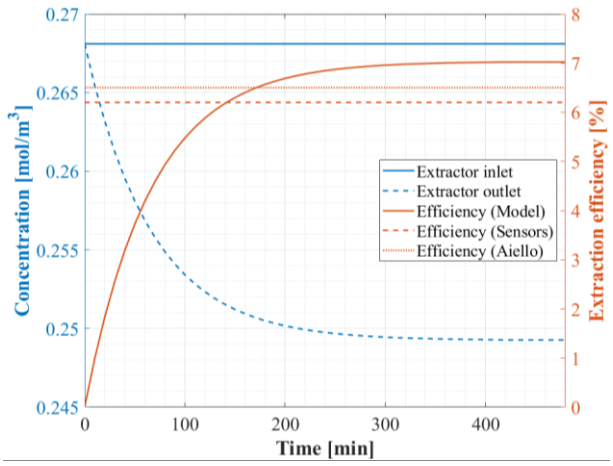

Fig. 2 Concentrations at extractor inlet and outlet and extraction efficiency compared with experimental ones.

It can be seen from the data in Table 4 that the efficiency resulting from the experiment varies in the range 6.2-6.5 %, whereas the model gives an efficiency equal to 7%, with relative errors varying from 7.4 to 11.4%. The average error is evaluated as:

$$e_{i,j} = 1 - \frac{\eta_j}{\eta_i} \qquad (11)$$

where i, j refer to the efficiency term with which the error is calculated. For instance, the error of the model efficiency referred to the efficiency measured by the permeation sensors is labelled as $e_{M,S}$.

Table 4. Comparison of model results with experiment.

Parameter	Description	Value
η_S	Extr. efficiency measured by sensors	6.2 [%]
η_{HGA}	Extr. efficiency measured by HGA	6.5 [%]
η_M	Extr. efficiency from the model	7.0 [%]
$e_{S,HGA}$	Error on efficiency sensors/HGA	4.8 [%]
$e_{M,S}$	Error on efficiency model/sensors	11.7 [%]
$e_{M,HGA}$	Error on efficiency model/HGA	7.4 [%]

The permeation fluxes, as shown in Table 5, are reported in terms of their average values. From calculations, it results that the trend is almost constant with respect to time, due to the continuous hydrogen injection in the saturator.

Table 5. Hydrogen permeation fluxes.

Parameter	Description	Value
Φ_p	Average perm. flux through pipes	$6.30 \cdot 10^{-8}$ [mol s^{-1}]
Φ_S	Average perm. flux through saturator	$1.07 \cdot 10^{-8}$ [mol s^{-1}]
Φ_E	Average perm. flux through extractor	$2.51 \cdot 10^{-8}$ [mol s^{-1}]

As shown in Fig. 6, most of the hydrogen permeation occurs in the pipes, 63.8%, whereas 36.2% in the saturator and in the extractor; the permeation flux in the extractor is almost twice the one in the saturator. The different values in the permeation fluxes can be explained by considering that the thickness of the pipes is nearly 1/3 the thickness of S200 and S300, whereas the difference between saturator and extractor may be due to the different modules of structured filling inserted (2 modules in the saturator, 4 modules in the extractor): hence, increasing the permeation area in extractor, the permeation flux tends to increase. The calculated ratio of hydrogen permeated (through pipes, saturator and extractor) to hydrogen extracted is equal to 9.76%. This means that the hydrogen losses through the plant are small if compared to the amount of hydrogen extracted in the mock-up.

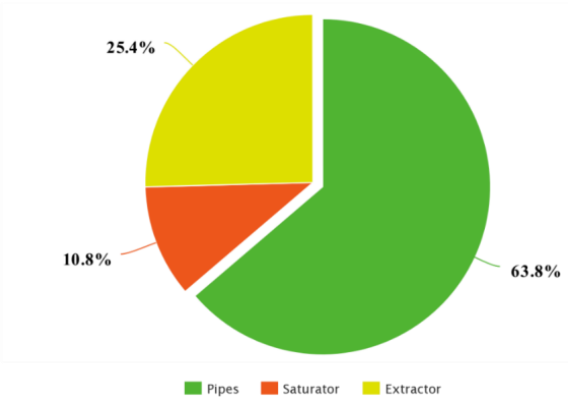

Fig 6. Permeation fluxes in TRIEX-II circuit.

5. Conclusions

In summary, a new multiscale model for the experimental facility TRIEX-II, installed at ENEA C.R. Brasimone Research Centre, was presented. This computational tool differs from other system level codes since it is able to describe the whole circuit with a 0D MATLAB/Simulink system level code, with the detail of the 2D sub-system constituted by the GLC mock-up, developed with COMSOL Multiphysics. Both the models adopted a diffusion-limited permeation regime.

From COMSOL, the velocity field of the LiPb inside the extractor was solved by means of the $k-\varepsilon$ turbulent model; a recirculation zone above the MellapakPlus and a finer dispersion of the liquid metal inside the structured filling were observed. The concentration profile along the packing is uniform, due to the uniform spatial distribution adopted for the sink term of Eq. 2. The study is limited by the lack of information on the sink term in the general transport equation. Notwithstanding this limitation, the study suggests that this approach can have the potential to be adapted for analyses of complex systems, at a multiscale level, in view of design improvements and safety-related issues for the tritium cycle of ITER – and in particular for the WCLL test blanket system – corroborating the results exposed in [5].

The whole Simulink model permitted to easily compare the extraction efficiency evaluated numerically with respect to the extraction efficiencies evaluated experimentally. In particular, as far as the experimental campaign is concerned, the extraction efficiency was determined by using hydrogen permeation sensors and a mass spectrometer, with the purpose of having two values coming from different measurement systems. The results from the model compared well with the experiment, giving a theoretical efficiency of 7% in spite of an experimental efficiency varying in the range 6.2-6.5%. The relative error varies in the range 7.4-11.4%. The permeation fluxes were evaluated theoretically, finding that almost 1/3 occurs in the piping and that the permeation flux in the extractor is nearly twice the one in the saturator. Finally, the hydrogen losses through the plant were small when compared to the amount of hydrogen extracted in the mock-up (9.76%).

An important question for future studies is to deeply investigate the spatial distribution of the sink term of the extractor mock-up. Further researches could also be conducted with the purpose of having experimental data on the permeation properties of the steels adopted for the piping and for the vessels of saturator and extractor.

Acknowledgements

The experimental set-up leading to this publication has been funded by Fusion for Energy under the contract F4E-FPA-372-SG04. The modelling activities of this publication reflect the views only of the authors, and Fusion for Energy cannot be held responsible for any use which may be made of the information contained therein.

References

[1] L. M. Giancarli, et al., Progress and challenges of the ITER TBM Program from the IO perspective, Fusion Engineering and Design 109-111 (2016) 1491-1497.

[2] M. Utili et al., Tritium Extraction From HCLL/WCLL/DCLL PbLi BBs of DEMO and HCLL TBS of ITER, IEEE Transactions on Plasma Science, 47 (2) (2019) 1464-1471.

[3] M. Utili, et al., Characterisation of Tritium Extraction Unit from Liquid Pb-15.7Li Alloy of WCLL-TBM in TRIEX-II Facility, Poster presented at the 14th International Symposium on Fusion Nuclear Technology, 22-27 September 2019, Budapest, Hungary.

[4] I. Ricapito, et al., Tritium technologies and transport modelling: main outcomes from the European TBM Project, Fusion Engineering and Design 136 (2018) 128-134.

[5] A. Ying, et al., Breeding blanket system design implications on tritium transport and permeation with high tritium ion implantation: A MATLAB/Simulink, COMSOL integrated dynamic tritium transport model for HCCR TBS retention in beryllium for tokamak plasma-facing applications, Fusion Engineering and Design 136 (2018) 1153-1160.

[6] MATLAB/Simulink. Version R2019a. Available online: http://www.mathworks.com/.

[7] COMSOL Multiphysics and Livelink for MATLAB. Version 5.4. Available online: http://www.comsol.com/.

[8] L. Candido, et al., Tritium transport model at the minimal functional unit level for HCLL and WCLL breeding blankets of DEMO, Fusion Engineering and Design 136 (2018) 1327-1331.

[9] F. Waelbroeck, et al., Influence of bulk and surface phenomena on the hydrogen permeation through metals, Berichte der Kernforschungsanlage Jülich 1966 (1984) 28-49.

[10] G. A. Esteban, et al., Hydrogen transport and trapping in EUROFER'97, Journal of Nuclear Materials 367 (2007) 473-477.

[11] K.S. Forcey, et al., Hydrogen transport and solubility in 316L and 1.4914 steels for fusion reactor applications, Journal of Nuclear Materials 160 (1988) 117-124.

[12] A. Aiello, et al., Determination of hydrogen solubility in lead lithium using SOLE device, Fusion Engineering and Design 81 (2006) 639-644.

[13] S.V. Stankus, et al., An experimental investigation of the density and thermal expansion of advanced materials and heat–transfer agents of liquid-metal systems of fusion reactor: lead–lithium eutectic, High Temperature, 44 (2006) 829-837.